

# Synthesis, characterization, and gas permeation properties of a hydrogen permeable silica membrane supported on porous alumina

D. Lee<sup>a</sup>, L. Zhang<sup>b</sup>, S.T. Oyama<sup>a,\*</sup>, S. Niu<sup>c</sup>, R.F. Saraf<sup>c</sup>

<sup>a</sup> Department of Chemical Engineering, Environmental Catalysis and Nanomaterials Laboratory,  
Virginia Polytechnic Institute and State University, Blacksburg, VA 24061, USA

<sup>b</sup> Department of Chemical Engineering, Nanjing University of Technology, Nanjing 210009, PR China

<sup>c</sup> Department of Chemical Engineering, Virginia Polytechnic Institute and State University, Blacksburg, VA 24061, USA

Received 13 March 2003; received in revised form 22 October 2003; accepted 30 October 2003

## Abstract

A highly hydrogen permselective composite silica membrane was obtained by depositing a thin silica layer on a porous alumina support by the chemical vapor deposition (CVD) of tetraethylorthosilicate (TEOS) at 873 K in inert gas at atmospheric pressure. The silica/alumina membrane showed a high hydrogen permeance ( $\sim 10^{-7}$  mol m<sup>-2</sup> s<sup>-1</sup> Pa<sup>-1</sup>) with selectivity over CH<sub>4</sub>, CO, and CO<sub>2</sub> in excess of 1000 at 873 K. Cross-sectional and surface images of the membranes obtained from scanning electron microscopy (SEM) and atomic force microscopy (AFM) showed that the silica film deposited on the  $\gamma$ -Al<sub>2</sub>O<sub>3</sub> support was uniform with a thickness of 20–30 nm. This indicated that the high temperature thermal decomposition of tetraethylorthosilicate (TEOS) used in this work was excellent in controlling the uniformity and thickness of the silica film formed on the porous alumina support. On the fresh alumina support the permeance of gases (He, H<sub>2</sub>, CH<sub>4</sub>, CO, and CO<sub>2</sub>) decreased with temperature and molecular weight in agreement with a Knudsen transport mechanism. However, on the silica/alumina membrane the permeation of H<sub>2</sub> and He was activated and increased with temperature. The transport mechanism for the small gas molecules (H<sub>2</sub> and He) through the silica membrane was analyzed using a permeation mechanism which involves the jumping of the diffusing molecules between adjacent solubility sites. The model analysis indicated that the structure of the silica layer is more open than that of vitreous silica glass, with larger interconnecting passageways and low activation energies for permeation, allowing for easier gas diffusion.

© 2003 Elsevier B.V. All rights reserved.

**Keywords:** Gas and vapor permeation; Inorganic membrane; Gas separation; AFM; SEM

## 1. Introduction

Hydrogen permeable and selective silica membranes have attracted much interest in the membrane gas separation field due to the importance of hydrogen as an industrial feedstock for the production of fuels and many chemicals [1,2]. Of particular interest has been the usage of hydrogen selective membranes for fuel cell applications [3]. Silica membranes are attractive since they are chemically and thermally stable while offering high permeability and selectivity for hydrogen [4]. Much research has been reported in recent years on the synthesis of silica membranes and their properties regarding hydrogen permeance and selectivity [5–15].

In our previous papers, we reported the synthesis and gas permeation properties of a highly hydrogen selective silica membrane which was obtained by depositing a thin silica layer on porous Vycor glass using the thermal decomposition of tetraethylorthosilicate at 873 K in an inert atmosphere [12,13]. The membrane obtained had an unprecedented high selectivity for hydrogen ( $\sim 10^4$ ) over CH<sub>4</sub>, CO, and CO<sub>2</sub> with permeance of hydrogen in the order of  $10^{-8}$  mol m<sup>-2</sup> s<sup>-1</sup> Pa<sup>-1</sup> at 873 K. However, the hydrogen permeance of this membrane was limited due to the low gas permeance of the Vycor membrane support itself at high temperatures.

The first silica membranes were obtained by placing a thin silica layer inside the pores of leached Vycor glass by means of a chemical vapor deposition (CVD) technique utilizing tetraethylorthosilicate (TEOS) [5,6]. The reaction was carried out at relatively low temperatures with water vapor [5] oxygen [6] or ozone [9] as coreactants and resulted in

\* Corresponding author. Tel.: +1-540-231-5309;

fax: +1-540-231-5022.

E-mail address: [oyama@vt.edu](mailto:oyama@vt.edu) (S.T. Oyama).

membranes with a high selectivity of 2000–3000 for hydrogen over nitrogen, but a relatively low permeability at 873 K of  $3.0 \times 10^{-9} \text{ mol m}^{-2} \text{ s}^{-1} \text{ Pa}^{-1}$ . These early membranes were limited by the pore structure of the Vycor glass support [5–9,12,13]. Improvement in permeability was obtained by preparing membranes using alumina supports [10,11,14,15] by sol gel [14,15] or chemical vapor deposition techniques [10,11]. The permeance of hydrogen in the CVD membranes at 873 K was  $7 \times 10^{-7} \text{ mol m}^{-2} \text{ s}^{-1} \text{ Pa}^{-1}$  but with selectivity over  $\text{N}_2$  of only 170 [11], while that in the sol gel membrane was  $5 \times 10^{-7} \text{ mol m}^{-2} \text{ s}^{-1} \text{ Pa}^{-1}$  at 473 K and with selectivity over  $\text{CO}_2$  of only 70 [15]. The sol gel membranes underwent loss of performance at high temperature through densification of the silica.

In this work we describe the synthesis of a highly hydrogen permeable silica membrane obtained by extending the CVD method to a porous alumina support. This membrane showed a high hydrogen permeance of the order of  $10^{-7} \text{ mol m}^{-2} \text{ s}^{-1} \text{ Pa}^{-1}$  at 873 K with selectivity of hydrogen over  $\text{CH}_4$ , CO, and  $\text{CO}_2$  above 1000. The notable result is that the permeance of hydrogen is one order of magnitude higher than that for the silica membrane obtained on the porous Vycor support in our previous work [13]. The membranes were examined using field emission scanning electron microscopy (FESEM) to give their cross-sectional morphology and atomic force microscopy (AFM) to show their surface structure. The gas permeation properties of the membranes were discussed, and the transport of He and  $\text{H}_2$  gases through the silica membrane was analyzed using a statistical gas permeation mechanism.

## 2. Experimental

The silica/alumina membrane was prepared by depositing a thin silica layer on a porous  $\gamma$ -alumina support by the thermal decomposition of tetraethylorthosilicate at 873 K in an argon stream. The membrane support used in this study was purchased from US Filter (Part No. S700-0011), and had a tubular geometry with an outside diameter of 10 mm and a thickness of 1.5 mm. This membrane support had a multilayered structure consisting of a coarse  $\alpha$ - $\text{Al}_2\text{O}_3$  tube coated with finer layers of  $\alpha$ - $\text{Al}_2\text{O}_3$  and an inner top layer of  $\gamma$ - $\text{Al}_2\text{O}_3$  of average 5 nm pore size. A 5 cm section of the alumina membrane support was connected at both ends to two pieces of dense alumina tubing using a high temperature glass glaze (Duncan, IN, Part No. 1001). Gas tight connections between the membrane support and the dense tubing were obtained after 0.5 h of thermal treatment at 1150 K.

After the joint connection, an additional  $\gamma$ - $\text{Al}_2\text{O}_3$  layer was introduced on top of the existing  $\gamma$ - $\text{Al}_2\text{O}_3$  layer of the alumina support to reduce defects or pinholes that give rise to a low hydrogen selectivity in the silica layer. A 0.05 M dispersion of boehmite ( $\gamma$ - $\text{AlOOH}$ ) sol was prepared following the method reported by Uhlhorn et al. [16]. Aluminum tri-*sec*-butoxide (Aldrich, 97%) was added to boiling wa-

ter with vigorous stirring, and 0.07 mol  $\text{HNO}_3$ /mol butoxide was added. This colloidal solution was boiled until most of the butanol was evaporated, then was refluxed for 20 h. Polyvinylalcohol (PVA, Fluka, MW 72 000) solution was prepared separately by adding 3.5 g of PVA to 100  $\text{cm}^3$  of boiling water followed by 5  $\text{cm}^3$  of 1 M  $\text{HNO}_3$ . The PVA solution was then refluxed for 4 h. A final 0.05 M boehmite sol was prepared after adding 660  $\text{cm}^3$  of the PVA solution per mol of boehmite followed by stirring for 3 h at 353 K. The inside of the alumina support tubing was dip coated with the 0.05 M boehmite sol for 10 s, dried for 24 h at room temperature, and then calcined at 873 K for 24 h (heating rate 1 K  $\text{min}^{-1}$ ).

Unsupported  $\gamma$ - $\text{Al}_2\text{O}_3$  films were also prepared by drying the boehmite sol in polypropylene Petri dishes at room temperature. The obtained gel films were calcined at the same temperature as used for the membrane synthesis (873 K) for various time (3, 24, 72 h) to determine the resulting pore size distributions of the  $\gamma$ - $\text{Al}_2\text{O}_3$ .

For the CVD of the silica layer, the alumina support substrate was installed concentrically inside another piece of glass tubing of 14 mm inside diameter using machined Swagelok fittings with Teflon ferrules. After placing the assembly in an electric furnace, argon gas flows were introduced on the outer shell side ( $19 \mu\text{mol s}^{-1}$ ) and inner tube side ( $15 \mu\text{mol s}^{-1}$ ) of the reactor (flow rates in  $\mu\text{mol s}^{-1}$  may be converted to  $\text{cm}^3 \text{ min}^{-1}$  (NTP) by multiplying by 1.5), and the temperature was raised to 873 K. A flow of tetraethylorthosilicate (Aldrich, 98%) was introduced on the inside of the porous alumina substrate through a bubbler (at 298 K) using argon ( $4 \mu\text{mol s}^{-1}$ ) as a carrier gas. This stream was mixed with the tube stream of argon before introducing it to the tube side to produce a stream with a TEOS concentration of  $0.02 \text{ mol m}^{-3}$  (0.045 mol%). The synthesis of the silica membrane was studied by varying the silica deposition time. The CVD process was interrupted at various times and the permeance of  $\text{H}_2$ ,  $\text{CH}_4$ , CO, and  $\text{CO}_2$  were measured at different deposition times at 873 K.

General gas permeation measurements were conducted in the temperature range 373–873 K by flowing  $40 \mu\text{mol s}^{-1}$  of a pure gas at 160 kPa through the inner tube. The permeation rate of each gas exiting from the shell side of the reactor assembly was measured with a sensitive bubble flow meter at atmospheric pressure. The permeance of gas was obtained from the expression  $Q_i = F_i / A \Delta P_i$ , where  $Q_i$  is the permeance ( $\text{mol m}^{-2} \text{ s}^{-1} \text{ Pa}^{-1}$ ) of species  $i$ ,  $F_i$  the gas flow rate on the shell side ( $\text{mol s}^{-1}$ ),  $A$  the surface area ( $\text{m}^2$ ) of the membrane section, and  $\Delta P_i$  the pressure difference (Pa) between the shell and tube side. For higher sensitivity the permeance of the gases was also measured with a gas chromatograph (GC) equipped with a thermal conductivity detector (SRI, Model 8610B). The tube side gas flow rates and pressure conditions were the same as above, however, on the shell side an argon flow was introduced as a sweep gas for the permeated gas. The shell side outlet gas flow rate was measured using a bubble flow meter, and the flow was

injected into the GC to obtain the concentration of the permeated gas. The permeance was then calculated using the outlet gas flow rate and the concentration of the permeated gas on the shell side.

Cross-sectional structures of the alumina support substrate and the silica membrane were characterized using a field emission scanning electron microscope (Leo 1550). The samples were prepared by mechanically breaking the membranes after putting them into liquid nitrogen for 60 s. The samples were then introduced into the electron microscope and coated with a layer of gold by sputtering. The multilayered structure of the alumina support membrane substrate was examined, and the thickness of the deposited silica layer of the silica membrane was obtained from high resolution cross-sectional photos. The inner surface structures of the fresh alumina support and silica membrane were also characterized using a multimode atomic force microscope (Digital Instrument, Nanoscope III). A cantilever with a pyramidal tip of Si (Nanoprobe) was used as the probe sensor. The surface structures of the samples were examined in the tapping mode to obtain the topography.

### 3. Results and discussion

The pore size distribution curves for the unsupported  $\gamma$ -Al<sub>2</sub>O<sub>3</sub> films obtained from nitrogen desorption isotherms using the Barrett, Joyner and Halenda (BJH) method are shown in Fig. 1. The results indicate that small pores were developed on the  $\gamma$ -Al<sub>2</sub>O<sub>3</sub> films with a pore size range between 3 and 5 nm after 3 h of calcination at 873 K. The size of the pores increased with further calcination (24 h) to give a narrow unimodal pore size distribution with average pore size of 4.5 nm. The pore size and its distribution changed little after extended calcination (72 h) indicating that the pore structure of the  $\gamma$ -Al<sub>2</sub>O<sub>3</sub> film became stable after 24 h.

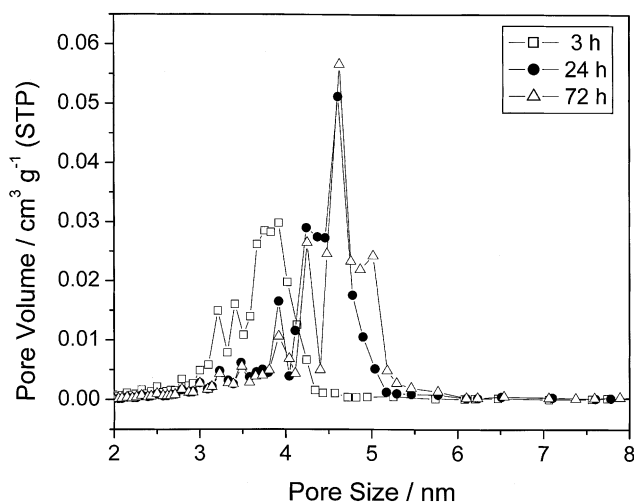


Fig. 1. Pore size distribution of the unsupported  $\gamma$ -Al<sub>2</sub>O<sub>3</sub> films.

#### 3.1. Gas transport property through the alumina support

The alumina membrane used in this study as a support for the silica membrane preparation had a graded multilayer structure with large macropores in the  $\alpha$ -Al<sub>2</sub>O<sub>3</sub> support layers to small mesopores on the top  $\gamma$ -Al<sub>2</sub>O<sub>3</sub> layer. The pore size of the support gradually decreased layerwise from a few  $\mu$ m to an average pore size of 4.5 nm for the top  $\gamma$ -Al<sub>2</sub>O<sub>3</sub> layer. The overall gas transport properties through this multilayered membrane were governed mainly by the transport properties of the top  $\gamma$ -Al<sub>2</sub>O<sub>3</sub> layer. This was due to the larger gas diffusion resistance imposed by the small pores of the top layer compared to those of the large pores of the supporting layers. In gas transport through porous materials, Knudsen diffusion is a well-known transport mechanism which occurs when the mean free path of gas molecules is much larger than the size of the pores [17]. In this regime, gas molecules diffuse through the pores by colliding with the pore walls under the driving force of a concentration gradient. The Knudsen permeance is given by

$$Q = \frac{\varepsilon d_p}{\tau L} \left( \frac{8}{9\pi MRT} \right)^{1/2} \quad (1)$$

where  $Q$  is the permeance ( $\text{mol m}^{-2} \text{s}^{-1} \text{Pa}^{-1}$ ),  $\varepsilon$  the porosity,  $d_p$  the pore diameter (m),  $\tau$  the tortuosity,  $L$  the membrane thickness (m),  $R$  the gas constant ( $8.314 \text{ J mol}^{-1} \text{K}^{-1}$ ),  $T$  the temperature (K), and  $M$  the molecular weight ( $\text{kg mol}^{-1}$ ). The Knudsen diffusion equation predicts that gas permeance will have an inverse square root dependency on both the molecular weight and temperature. The ratio of the mean free paths of the gases used in this work (He, H<sub>2</sub>, CH<sub>4</sub>, CO, and CO<sub>2</sub>) and the pore size of the  $\gamma$ -Al<sub>2</sub>O<sub>3</sub> layer falls between 30 and 120, therefore the gas transport is expected to show Knudsen permeation characteristics.

The experimental gas permeance through the alumina membrane support was plotted versus the inverse square root of molecular weight at various temperatures, and the linear regression fits are presented in Fig. 2. The results show a good linear dependence ( $r^2 = 0.997$ – $0.999$ ) confirming that the gas transport occurred mainly by Knudsen diffusion. The hydrogen selectivities over other gases (He: 1.36, CH<sub>4</sub>: 2.40, CO: 3.25, and CO<sub>2</sub>: 4.22) showed good agreement with the theoretical Knudsen selectivity values (He: 1.41, CH<sub>4</sub>: 2.82, CO: 3.72, and CO<sub>2</sub>: 4.67). The slightly lower experimental values for CH<sub>4</sub>, CO and CO<sub>2</sub> are likely due to a small contribution of surface diffusion for these condensable gases [13]. The permeance data was also plotted versus the inverse square root of the temperature and the linear regression fits are presented in Fig. 3. The results again show good fits ( $r^2 = 0.930$ – $0.995$ ) following the behavior expected from Knudsen transport.

#### 3.2. Gas transport property through the silica membrane

The evolution of the gas permeance on the silica membrane was measured at 873 K as a function of the silica

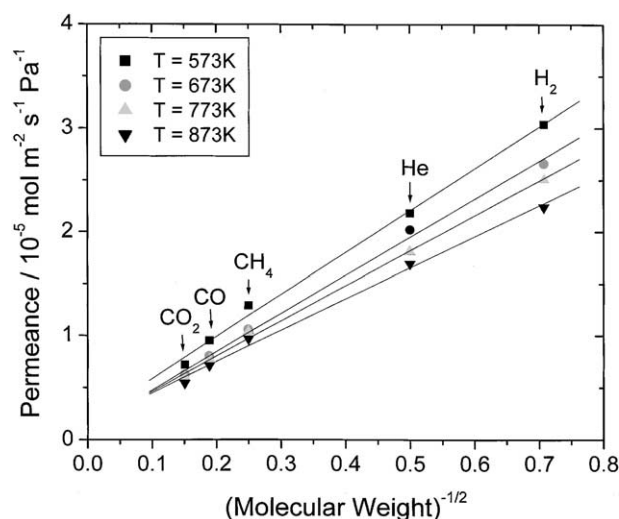


Fig. 2. Gas permeance vs. molecular weight<sup>-1/2</sup> for the fresh alumina support.

deposition time to monitor the formation of the silica layer on the membrane support. The results are shown in Fig. 4. Initially, the fresh alumina support showed very high permeance for all of the gases ( $H_2 = 2.2 \times 10^{-5} \text{ mol m}^{-2} \text{ s}^{-1} \text{ Pa}^{-1}$ ,  $CH_4 = 9.7 \times 10^{-6} \text{ mol m}^{-2} \text{ s}^{-1} \text{ Pa}^{-1}$ ,  $CO = 7.1 \times 10^{-6} \text{ mol m}^{-2} \text{ s}^{-1} \text{ Pa}^{-1}$ ,  $CO_2 = 5.4 \times 10^{-6} \text{ mol m}^{-2} \text{ s}^{-1} \text{ Pa}^{-1}$ ). The permeance of all the gases decreased with silica deposition time. For hydrogen, the permeance decreased rapidly after 3 h of silica deposition to the order of  $10^{-7} \text{ mol m}^{-2} \text{ s}^{-1} \text{ Pa}^{-1}$ , and then decreased slowly with further silica deposition. In contrast, the permeance of  $CH_4$ ,  $CO$ , and  $CO_2$  showed a continuous and rapid drop with silica deposition. After 12 h of deposition the permeance of hydrogen remained at  $1.2 \times 10^{-7} \text{ mol m}^{-2} \text{ s}^{-1} \text{ Pa}^{-1}$ , whereas the permeance of other gases dropped off significantly ( $CH_4 = 4.3 \times 10^{-11} \text{ mol m}^{-2} \text{ s}^{-1} \text{ Pa}^{-1}$ ,

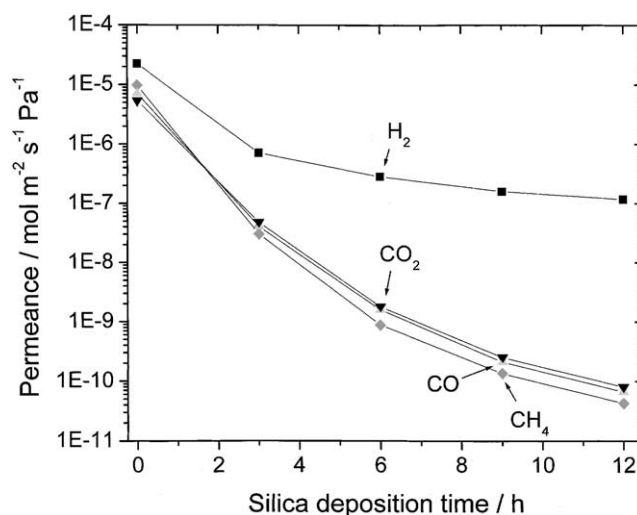


Fig. 4. Gas permeance vs. silica deposition time.

$CO = 6.7 \times 10^{-11} \text{ mol m}^{-2} \text{ s}^{-1} \text{ Pa}^{-1}$ ,  $CO_2 = 8.0 \times 10^{-11} \text{ mol m}^{-2} \text{ s}^{-1} \text{ Pa}^{-1}$ ). The results indicate that a complete silica layer was formed on the alumina support after 12 h of deposition, and that the layer was selective for  $H_2$  transport while significantly excluding passage of  $CH_4$ ,  $CO$ , and  $CO_2$  through the membrane. Before the silica deposition, the permeance order of the gases through the alumina support was  $H_2 > CH_4 > CO > CO_2$  showing an inverse dependence on the molecular weight of the gases, in agreement with the Knudsen diffusion mechanism. However, after 3 h of silica deposition the permeance order changed to  $H_2 > CO_2 > CO > CH_4$ , which followed molecular size ( $H_2 = 0.289 \text{ nm}$ ,  $CO_2 = 0.33 \text{ nm}$ ,  $CO = 0.376 \text{ nm}$ ,  $CH_4 = 0.38 \text{ nm}$  [18]), and this order was retained with further silica deposition. This gives evidence that the mechanism of molecular differentiation by the silica layer is through size selectivity.

The hydrogen selectivity over other gases is shown as a function of hydrogen permeance in Fig. 5. The selectivity

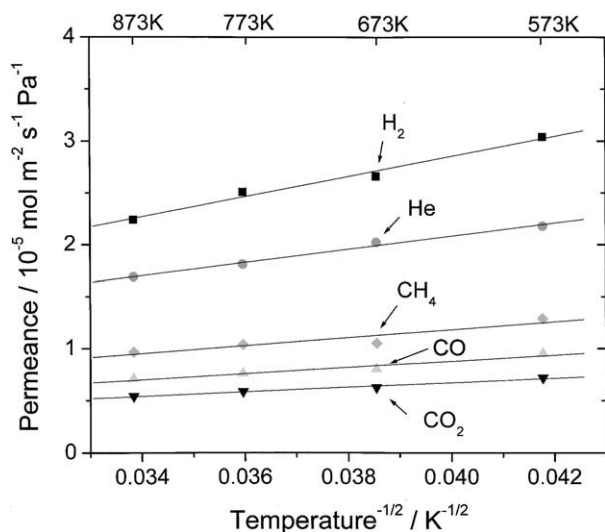


Fig. 3. Gas permeance vs. temperature<sup>-1/2</sup> for the fresh alumina support.

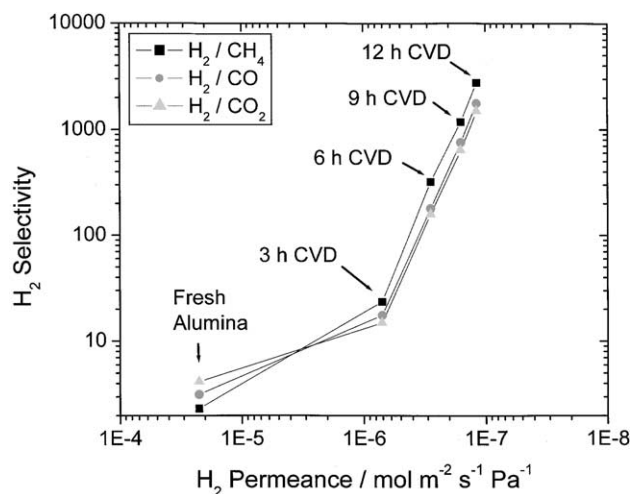


Fig. 5. Selectivity of hydrogen vs.  $H_2$  permeance.



for hydrogen on the fresh alumina support was low for all the gases. As discussed in the previous section, the selectivity was characteristic of Knudsen diffusion. After 3 h of silica deposition the selectivity for hydrogen showed a slight increase accompanied by a large decrease in  $H_2$  permeance from the order of  $10^{-5}$  to  $10^{-7}$   $\text{mol m}^{-2} \text{s}^{-1} \text{Pa}^{-1}$ . The  $H_2$  selectivity then increased rapidly with further silica deposition, with only a small drop in hydrogen permeance. In this regime the increase of  $H_2$  selectivity followed a log linear relation with the silica deposition. After 12 h of silica deposition the hydrogen selectivity of the membrane increased to over 1000 for all the gases ( $\text{CH}_4$ : 2800,  $\text{CO}$ : 1800,  $\text{CO}_2$ : 1500).

The temperature dependence of small gas transport through the silica membrane obtained after 12 h of silica deposition was investigated by measuring the permeance of  $H_2$  and He at various temperatures (373–873 K). It was found that the permeance of these gases through the silica membrane was activated, and increased with temperature. This differed from the permeance in the fresh alumina membrane support where the permeance decreased with temperature accordance with the Knudsen transport mechanism. The permeance order of these gases ( $\text{He} > H_2$ ) followed molecular size ( $\text{He} = 0.26 \text{ nm}$ ,  $H_2 = 0.289 \text{ nm}$  [18]) rather than the mass of the molecules ( $\text{He} = 4.0 \text{ a.u.}$ ,  $H_2 = 2.01 \text{ a.u.}$ ). The activation energies of permeation were obtained by fitting the experimental gas permeance data to an Arrhenius expression

$$Q = Q_0 \exp\left(\frac{-E_a}{RT}\right) \quad (2)$$

where  $Q$  is the permeance,  $Q_0$  the pre-exponential factor ( $\text{mol m}^{-2} \text{s}^{-1} \text{Pa}^{-1}$ ),  $E_a$  the activation energy ( $\text{J mol}^{-1}$ ),  $R$  the gas constant ( $8.314 \text{ J mol}^{-1} \text{K}^{-1}$ ), and  $T$  the temperature (K). The fitting results and associated parameter values are shown in Fig. 6 and Table 1. The experimental permeance

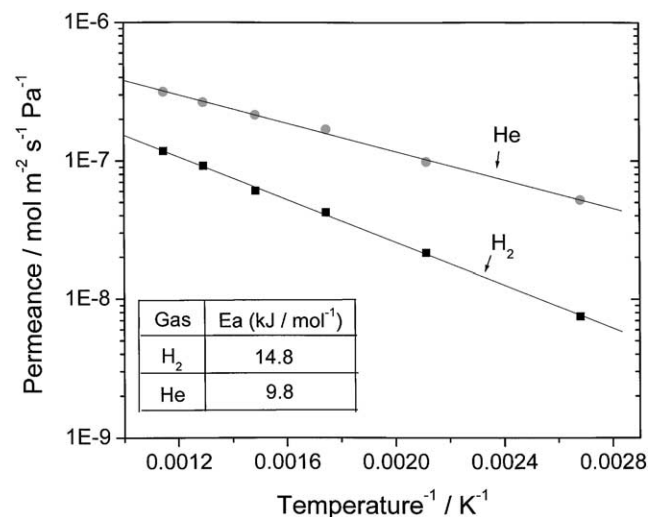


Fig. 6. Arrhenius plot for the permeance of  $H_2$  and He on the silica membrane.

Table 1

Best-fit pre-exponential factor and activation energy for the Arrhenius gas permeation equation

Gas	Pre-exponential factor, $Q_0$ ( $\text{mol m}^{-2} \text{s}^{-1} \text{Pa}^{-1}$ )	Activation energy, $E_a$ ( $\text{kJ mol}^{-1}$ )	Sum of least squares, $\sum(Q_{\text{calc.}} - Q_{\text{expl.}})^2$
$H_2$	$9.0 \times 10^{-7}$	14.8	$1.9 \times 10^{-17}$
He	$1.2 \times 10^{-6}$	9.8	$1.8 \times 10^{-16}$

data show good fits to the Arrhenius expression with an activation energy for  $H_2$  of  $14.8 \text{ kJ mol}^{-1}$  and for He of  $9.8 \text{ kJ mol}^{-1}$ .

### 3.3. Characterization of the membranes

The cross-sectional images of the fresh alumina support and the silica membrane obtained by high resolution field emission scanning electron microscopy are shown in Fig. 7(a)–(d). The cross-sectional photo of the fresh alumina support in Fig. 7(a) shows the multilayered graded structure of the support with different particle sizes for each  $\text{Al}_2\text{O}_3$  layer, where the particle and pore size decrease gradually from the bottom of the figure (outside of the tube) to the top (inside of the tube). The top  $\gamma\text{-Al}_2\text{O}_3$  layer with an average pore size of  $4.5 \text{ nm}$  had a thickness of about  $4\text{--}5 \mu\text{m}$ . Fig. 7(b) is a magnified photo of the top  $\gamma\text{-Al}_2\text{O}_3$  layer of the fresh alumina support.

The cross-sectional structure of the silica membrane is shown in Fig. 7(c) and (d). The figures show a silica layer with a thickness of about  $20\text{--}30 \text{ nm}$  formed on top of the  $\gamma\text{-Al}_2\text{O}_3$  layer after 12 h of silica deposition. The deposited silica layer shows good uniformity with a clear boundary with the support  $\gamma\text{-Al}_2\text{O}_3$  layer. However, the cross-sectional morphology of the support  $\gamma\text{-Al}_2\text{O}_3$  layer for the silica membrane is different from that of the fresh alumina support toward the bottom. This may have been caused by the alteration of the fracture properties of the  $\gamma\text{-Al}_2\text{O}_3$  by the silica.

The surface structures of the fresh alumina support obtained from AFM measurements are shown in Fig. 8(a)–(c). Fig. 8(a) and (b) are phase images of the  $\gamma\text{-Al}_2\text{O}_3$  surface with scan sizes of  $500 \text{ nm} \times 500 \text{ nm}$  and  $250 \text{ nm} \times 250 \text{ nm}$ , respectively, and Fig. 8(c) is the surface height image for Fig. 8(a). The phase images for the fresh alumina support show that the surface structure of the  $\gamma\text{-Al}_2\text{O}_3$  layer has a rough and jagged topography with randomly distributed  $\gamma\text{-Al}_2\text{O}_3$  particles. The size of the particles is not uniform, and has an approximate size range of  $20\text{--}40 \text{ nm}$ . Close examination of Fig. 8(b) indicates that the pore entrances are formed from the contact between three or four particles. The surface height image, Fig. 8(c), shows a three dimensional view of the surface. The image confirms that the topography of the surface is rough and uneven in the scale of nanometers. The surface shows many sharp peaks and deep valleys, as would be expected for particles deposited on a surface.

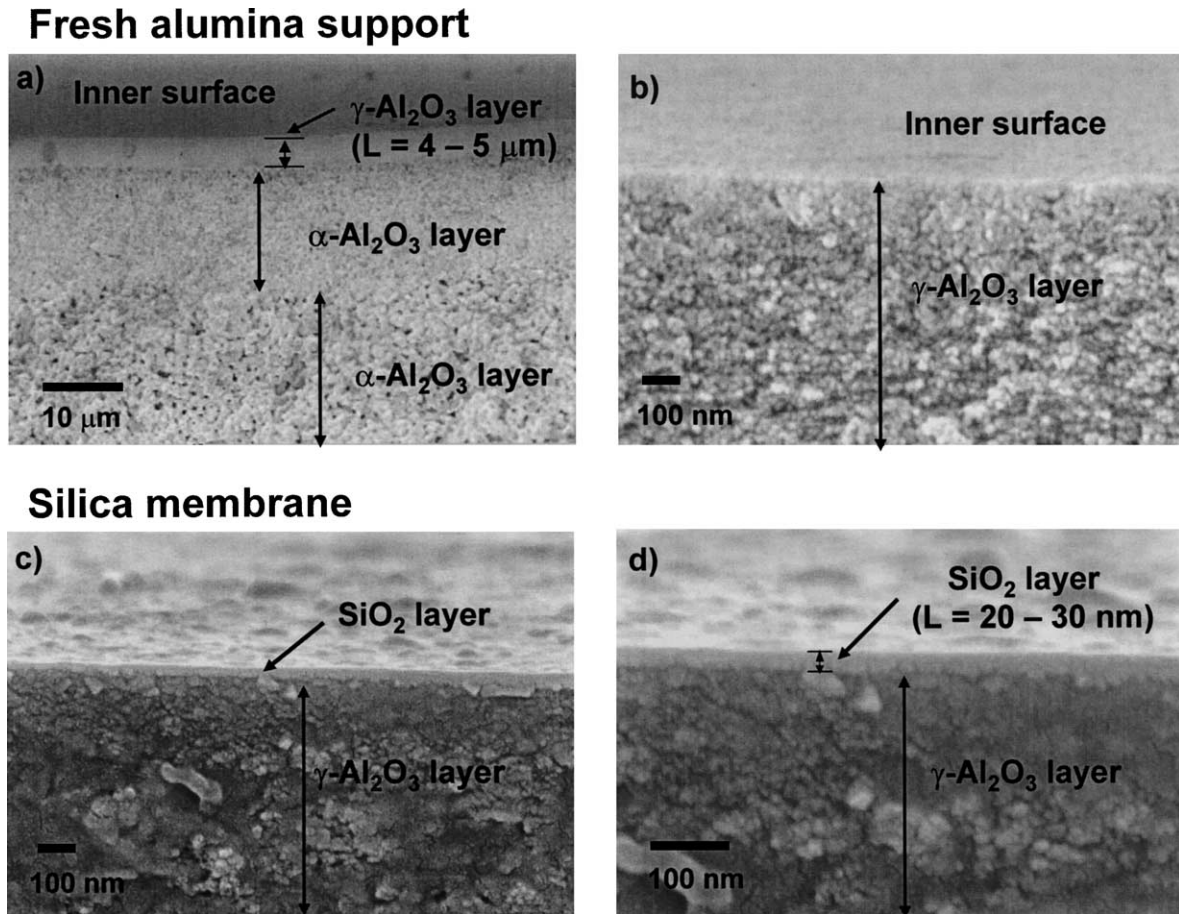


Fig. 7. SEM cross-sectional photos of the fresh alumina support and the silica membrane: (a) fresh alumina support (magnification = 2000×); (b) fresh alumina support (magnification = 100 000×); (c) silica membrane (magnification = 100 000×); (d) silica membrane (magnification = 200 000×).

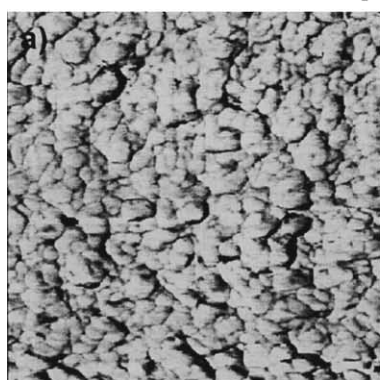
The surface structure of the silica membrane after 12 h of silica deposition is shown in Fig. 8(d)–(f). Fig. 8(d) and (e) are phase images with scan size of 500 nm × 500 nm and 250 nm × 250 nm, respectively, and Fig. 8(f) is a surface height image for the surface displayed in Fig. 8(d). The phase images show that the surface structure is smoother compared to that of the fresh  $\gamma$ - $\text{Al}_2\text{O}_3$  surface showing rounded particles due to the presence of the thin silica layer. The surface height image, Fig. 8(f), clearly indicates a change of surface topography for the silica membrane, and also shows that the particles have become larger and smoother. The roughness of the surface structure decreased after silica deposition showing shallower peaks and valleys. To compare the roughness of the surfaces the standard deviation of the height for the fresh alumina support and silica membrane surface was calculated by randomly taking eight cross-sections of the surface height images (Fig. 8(c) and (f)). The standard deviation ( $\sigma$ ) of the height is defined as

$$\sigma = \sqrt{\frac{\sum (Z_i - Z_{\text{ave}})^2}{N}} \quad (3)$$

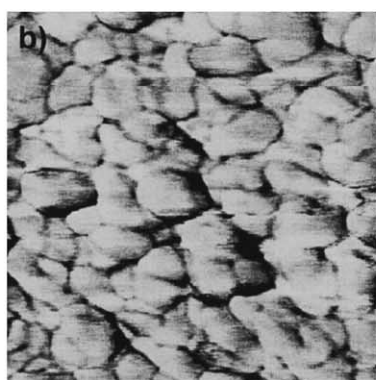
where  $Z_i$  is the height of peaks or valleys for the  $i$ th data point,  $Z_{\text{ave}}$  the average height, and  $N$  the total number of

data points. The calculated values were  $\sigma = 5.4$  nm for the fresh alumina support surface and  $\sigma = 3.7$  nm for the silica membrane surface. The results give a quantitative measure of the change of the surface roughness due to the deposition of the silica layer on the fresh  $\gamma$ - $\text{Al}_2\text{O}_3$  layer. The decrease of the surface roughness of the alumina surface with the silica layer gives insight about the nature of the deposition process. Schematic representations of the topography of the deposited layer are given in Fig. 9(a)–(c). Fig. 9(a) shows the peaks and valleys of the alumina surface before silica deposition. Fig. 9(b) shows the surface with the silica layer in the case where deposition was uniform due to the flux of the CVD species in the direction normal to the surface. For this situation the thickness of the overlayer would be expected, so the  $\sigma$  value should remain constant. Fig. 9(c) show the case where preferential layer growth occurs in the valleys. The result is a smoothing of the roughness of the surface and a decrease in the  $\sigma$  value. In fact, this is what is observed experimentally, and the result is reasonable. The average coordination at the sites in the valleys is higher than in the peaks, resulting in a larger number of bonding interaction as the silicate precursors are deposited. Conversely at the peaks the average coordination number is lower than

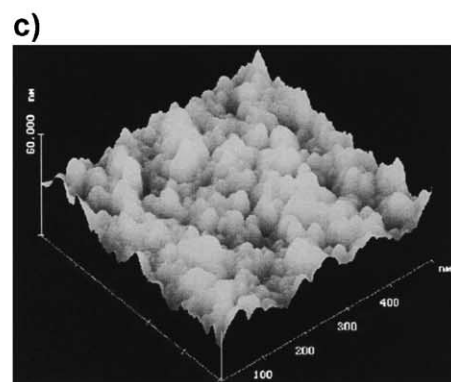
## Fresh alumina support



500 × 500 nm<sup>2</sup>

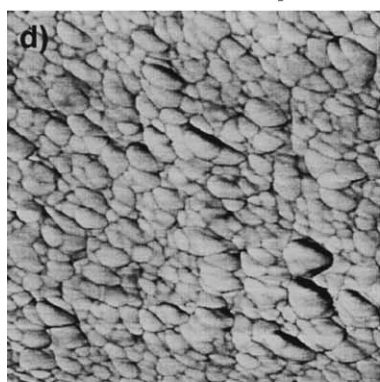


250 × 250 nm<sup>2</sup>

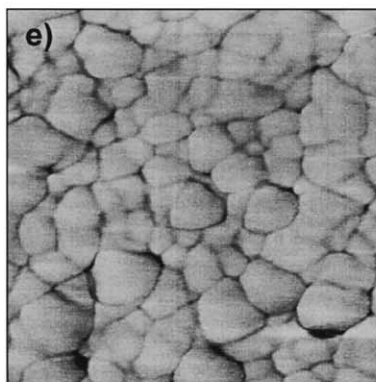


500 × 500 nm<sup>2</sup>

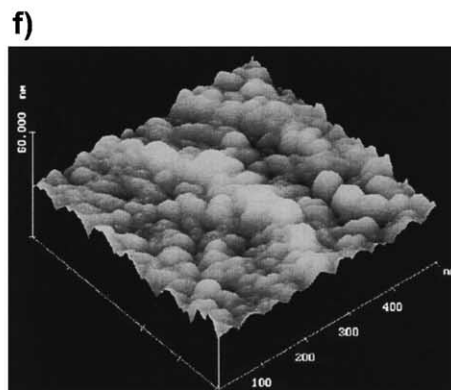
## After silica deposition



500 × 500 nm<sup>2</sup>

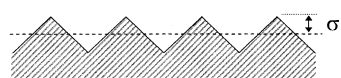


250 × 250 nm<sup>2</sup>

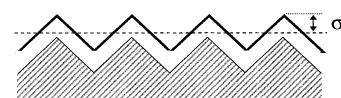


500 × 500 nm<sup>2</sup>

Fig. 8. AFM images of the surface of the fresh  $\gamma$ - $\text{Al}_2\text{O}_3$  and the silica membrane: (a) and (b) phase image of the surface of the fresh alumina support; (c) height image of the surface of the fresh alumina surface; (d) and (e) phase image of the surface of the silica membrane; (f) height image of the surface of the silica membrane.



(a) Fresh alumina surface



(b) Uniform deposition



(c) Preferential deposition

Fig. 9. Schematic representations of uniform and preferential film deposition.

in the valleys resulting in destabilization of the silica film precursors. These effects give rise to preferential filling of the valley sites. This mechanism also suggests that there is some mobility of the silica species as they are deposited on the surface of the membrane.

### 3.4. Mechanism of $\text{H}_2$ and $\text{He}$ permeation through the silica membrane

In a previous study [13], we showed that the gas permeation characteristics through the silica membrane layer obtained by CVD on a porous Vycor support were similar to those for vitreous silica glasses. It was found in that work that a uniform and defect-free silica layer was formed by CVD which allowed permeation of only gas molecules of small size ( $\text{He} = 0.26 \text{ nm}$ ,  $\text{Ne} = 0.275 \text{ nm}$ ,  $\text{H}_2 = 0.289 \text{ nm}$  [18]) while excluding the transport of gas molecules of large dimensions ( $\text{CO}_2 = 0.33 \text{ nm}$ ,  $\text{CO} = 0.376 \text{ nm}$ ,  $\text{CH}_4 = 0.38 \text{ nm}$ ). This could be explained from the structure of vitreous silica glasses which had been described as a disordered form of  $\beta$ -cristobalite that contains 5–8 membered rings, in



which solubility sites are approximately 0.3 nm in diameter [19]. The restricted size of the solubility sites in the silica matrix structure allows sorption of the small gas molecules while restricting sorption of the large gas molecules by size differentiation. The mechanism of small gas transport through the silica membrane is molecular diffusion, in which gas molecules adsorb in the solubility sites and then diffuse through the silica structure by jumping to adjacent solubility sites under the driving force of a concentration gradient. A few studies have been reported in the literature describing the sorption and diffusion of small molecules in silica glass using a statistical mechanics approach [20–22]. A monatomic gas permeance equation for silica glass has been presented [20]:

$$Q = \frac{1}{6L} \left( \frac{d^2}{h} \right) \left( \frac{h^2}{2\pi mkT} \right)^{3/2} \times \frac{N_s/N_A}{(e^{h\nu^*/2kT} - e^{-h\nu^*/2kT})^2} e^{-\Delta E_K/RT} \quad (4)$$

where  $Q$  is the permeance ( $\text{mol m}^{-2} \text{s}^{-1} \text{Pa}^{-1}$ ),  $L$  the thickness of the diffusion layer (m),  $d$  the jump distance (m),  $h$  the Plank's constant,  $k$  the Boltzmann's constant,  $m$  the mass of the molecules,  $N_s$  the number of solubility sites available/ $\text{m}^3$  of glass volume,  $N_A$  the Avogadro's number,  $\nu^*$  the vibrational frequency of the gas molecules at the doorway sites,  $R$  the gas constant,  $T$  the temperature, and  $\Delta E_K$  the activation energy for permeation. This permeance model can be applied to hydrogen in a similar form taking into account loss of rotational freedom at the doorway sites through a factor  $(\sigma h^2/\sqrt{8\pi kT})^{0.2}$ , where  $\sigma$  is the symmetry factor (2) for  $\text{H}_2$ ,  $I$  is its moment of inertia, and the exponent, 0.2, is empirical [23].

The experimental permeance of He and  $\text{H}_2$  through the silica membrane obtained in this study was analyzed using the gas permeance equation respectively without and with correction for rotational freedom (Eq. (4)). The model equation has three adjustable parameters: the number of solubility sites,  $N_s$ , the vibrational frequency of molecules at the doorway sites,  $\nu^*$ , and the activation energy for permeation ( $\Delta E_K$ ). A three-parameter optimization was carried out for  $N_s$ ,  $\nu^*$ , and  $\Delta E_K$  to find the best-fit parameter values for the experimental gas permeance data. An optimization program was written in Fortran using Newton's method [24]. The thickness of the silica layer,  $L$ , used was 30 nm which was obtained from the SEM experiments. The jump distance,  $d$ , was obtained from a correlation with the number of solubility sites [23]. The results of the numerical fitting are presented in Fig. 10. The calculations show excellent agree-

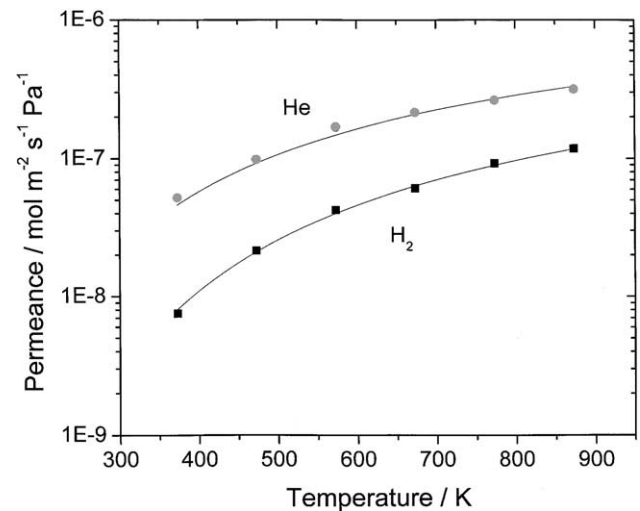


Fig. 10. He and  $\text{H}_2$  permeances obtained by the solubility site mechanism: points, experimental values; curves, calculated values.

ment between the model analysis and experimental permeance data with a permeance order of  $\text{He} > \text{H}_2$  which is the same as that for silica glass [25–28]. This is an unusual order from the standpoint of Knudsen diffusion as the molecular weight of He (4.0 a.u.) is twice as large as that of  $\text{H}_2$  (2.01 a.u.), but is well explained by the jump mechanism. Basically, the smaller size of He allows its accommodation in a larger number of solubility sites than  $\text{H}_2$  and also results in a smaller jump barrier. The results of the calculations are detailed in the following paragraph.

The best-fit parameter values in the solubility site equation are summarized in Table 2. The calculated vibrational frequency values at the doorway sites ( $\nu^*$ ) were  $8.10 \times 10^{12} \text{ s}^{-1}$  for hydrogen and  $7.77 \times 10^{12} \text{ s}^{-1}$  for helium, which are close to the vibrational frequency values at the solubility sites for silica glass reported in the literature ( $\text{H}_2 = 1.22 \times 10^{13} \text{ s}^{-1}$ ,  $\text{He} = 6.90 \times 10^{12} \text{ s}^{-1}$  [22]). The calculated  $N_s$  values were  $2.73 \times 10^{26}$  sites  $\text{m}^{-3}$  for hydrogen and  $7.40 \times 10^{26}$  sites  $\text{m}^{-3}$  for helium, which are slightly lower than those reported for vitreous silica glass ( $\text{H}_2 = 1.07 \times 10^{27}$  sites  $\text{m}^{-3}$  [29],  $\text{He} = 2.22 \times 10^{27}$  sites  $\text{m}^{-3}$  [30]). This makes sense since the structure of the silica layer formed by CVD in this work is expected to be less dense than vitreous silica. Note that the value of  $N_s$  is larger for He than for  $\text{H}_2$ . This is because on the average there are more sites that are able to accommodate the smaller He atom than the slightly larger  $\text{H}_2$  molecule. The calculated activation energies ( $\text{H}_2 = 12.8 \text{ kJ mol}^{-1}$ ,  $\text{He} = 8.0 \text{ kJ mol}^{-1}$ ) were

Table 2

Best-fit model parameters for the solubility site equation (based on 30 nm of the silica layer thickness)

Gas	Number of solubility sites, $N_s$ ( $\text{m}^{-3}$ )	Vibrational frequency, $\nu^*$ ( $\text{s}^{-1}$ )	Activation energy, $\Delta E_K$ ( $\text{kJ mol}^{-1}$ )	Sum of least squares, $\sum(Q_{\text{calc.}} - Q_{\text{expl.}})^2$
$\text{H}_2$	$2.73 \times 10^{26}$	$8.10 \times 10^{12}$	12.8	$1.95 \times 10^{-17}$
He	$7.40 \times 10^{26}$	$7.77 \times 10^{12}$	8.0	$8.09 \times 10^{-16}$



also in good agreement with the measured values ( $H_2 = 14.8 \text{ kJ mol}^{-1}$ ,  $He = 9.8 \text{ kJ mol}^{-1}$ ). The activation energies for small gas permeation through the silica layer obtained in this work are much lower than those for the vitreous silica glass reported in the literature ( $H_2 = 37.2\text{--}38.3 \text{ kJ mol}^{-1}$  [25,26],  $He = 17.8\text{--}21.1 \text{ kJ mol}^{-1}$  [27,28]), indicating that the doorway passageways in the silica layer are larger. The larger permeability of He over  $H_2$  can thus be understood from the larger number of solubility sites for He, coupled with a lower jump barrier.

In summary, the results of this study indicated that the interstitial structure of silica obtained by CVD in this membrane is more open than in vitreous glass, and thus offers easier diffusion of small gas molecules, resulting in high permeances for  $H_2$  and He. The jump analysis gave good simulated permeance results with physically realistic values for the number of solubility sites, vibrational frequency, and activation energy, which matched very well with experimental data.

#### 4. Conclusions

A silica membrane was prepared on a porous alumina support by thermal decomposition of a silica precursor at 873 K in an inert atmosphere. After 12 h of silica deposition, the resulting composite membrane showed a high hydrogen permeance of the order of  $10^{-7} \text{ mol m}^{-2} \text{ s}^{-1} \text{ Pa}^{-1}$  at 873 K with  $H_2$  selectivities over  $CH_4$ , CO, and  $CO_2$  in excess of 1000. The gas permeance through the alumina support decreased with the inverse square root of temperature in accordance with a Knudsen permeation mechanism. The small gas permeance ( $He$ , and  $H_2$ ) through the silica/alumina membrane was activated, and increased with temperature, and could be explained quantitatively by a jump mechanism between solubility sites. The thickness of the silica layer obtained from FESEM experiments was about 20–30 nm. The surface structure of the membranes obtained by AFM measurements indicated that the surface became smooth after the silica layer deposition indicating a uniform silica film formation on the  $\gamma\text{-Al}_2\text{O}_3$  surface of the alumina support. These results indicate that the high temperature chemical vapor deposition of silica by the thermal decomposition of TEOS applied in this work is excellent in controlling the thickness and uniformity of the silica layer formed on porous supports. The mechanism of small gas permeation through the silica membrane was described by a permeance model originally presented for silica glass. The model analysis results gave good agreement with experimental gas permeance data using physically realistic values for the number of solubility sites ( $N_s$ ), vibrational frequency of the molecules at the doorway sites ( $\nu^*$ ), and activation energy of permeation. The lower values in the number of solubility sites and low activation energies for the silica layer in this work compared to those for vitreous silica glasses indicated that the interstitial structure of the silica obtained from CVD is less

dense, thus providing higher diffusivity. These give rise to high permeance for  $H_2$  and He with hydrogen selectivities for  $CH_4$ , CO, and  $CO_2$  over 1500 at 873 K.

#### Acknowledgements

The authors thank Stephen McCartney for his help with the FESEM measurements. The authors also thank the Director, National Science Foundation, Division of Chemical and Thermal Systems through Grant No. CTS-0321979 and ConocoPhillips for support of this research.

#### References

- [1] R. Ramachandran, R.K. Menon, An overview of industrial uses of hydrogen, *Int. J. Hydrogen Energy* 23 (1998) 593.
- [2] T.N. Veziroglu, Hydrogen energy system as a permanent solution to global energy—environmental problems, *Chem. Ind.* 53 (1999) 383.
- [3] Novel fuel processor targets fuel-cell commercialization, *Chem. Eng. Prog.* (November 2002) 13.
- [4] A.J. Bugggraaf, L. Cot, *Fundamentals of Inorganic Membrane Science and Technology*, Elsevier, Amsterdam, 1996.
- [5] G.R. Gavalas, C.E. Megiris, S.W. Nam, Deposition of  $H_2$ -permselective  $SiO_2$  films, *Chem. Eng. Sci.* 44 (9) (1989) 1829.
- [6] T. Okubo, H. Inoue, Introduction of specific gas selectivity to porous glass membranes by treatment with tetraethoxysilane, *J. Membr. Sci.* 42 (1989) 109.
- [7] H.Y. Ha, S.W. Nam, S.-A. Hong, W.K. Lee, Chemical vapor deposition of hydrogen-permselective silica films on porous glass supports from tetraethylorthosilicate, *J. Membr. Sci.* 85 (1993) 279.
- [8] R.A. Levy, E.S. Ramos, L.N. Krasnoperov, A. Datta, J.M. Grow, Microporous  $SiO_2$ /Vycor membranes for gas separation, *J. Mater. Res.* 11 (1996) 3164.
- [9] S.-I. Nakao, T. Suzuki, T. Sugawara, T. Tsuru, S. Kimura, Preparation of microporous membranes by TEOS/ $O_3$  CVD in the opposing reactants geometry, *Micropor. Mesopor. Mater.* 37 (2000) 145.
- [10] S. Morooka, S. Yan, K. Kusakabe, Y. Akiyama, Formation of hydrogen-permselective  $SiO_2$  membrane in macropores of  $\alpha$ -alumina support tube by thermal decomposition of TEOS, *J. Membr. Sci.* 101 (1995) 9.
- [11] B.K. Sea, K. Kusakabe, S. Morooka, Pore size control and gas permeation kinetics of silica membranes by pyrolysis of phenyl-substituted ethoxysilanes with cross-flow through a porous support wall, *J. Membr. Sci.* 130 (1997) 41.
- [12] S.T. Oyama, D. Lee, S. Sugiyama, K. Fukui, Y. Iwasawa, Characterization of a highly selective hydrogen permeable silica membrane, *J. Mater. Sci.* 36 (2001) 5213.
- [13] D. Lee, S.T. Oyama, Gas permeation characteristics of a hydrogen selective supported silica membrane, *J. Membr. Sci.* 210 (2002) 291.
- [14] B.N. Nair, T. Yamaguchi, T. Okubo, H. Suematsu, K. Keizer, S.-I. Nakao, Sol-gel synthesis of molecular sieving silica membranes, *J. Membr. Sci.* 135 (1997) 237.
- [15] R.M. de Vos, H. Verweij, High-selective, high-flux silica membranes for gas separation, *Science* 279 (1998) 1710.
- [16] R.J.R. Uhlhorn, M.H.B.J. Huis In't Veld, K. Keizer, A.J. Burggraaf, Synthesis of ceramic membranes. Part I. Synthesis of non-supported and supported  $\gamma$ -alumina membranes without defects, *J. Mater. Sci.* 27 (1992) 527.
- [17] M. Knudsen, The law of the molecular flow and viscosity of gases moving through tubes, *Ann. Phys.* 28 (1909) 75.

- [18] D.W. Breck, Zeolite Molecular Sieves: Structure, Chemistry and Use, Wiley, New York, 1974, p. 636.
- [19] R.M. Barrer, D.E.W. Vaughan, Solution and diffusion of helium and neon in tridymite and cristobalite, *Trans. Faraday Soc.* 63 (1967) 2275.
- [20] J.S. Masaryk, R.M. Fulrath, Diffusivity of helium in fused silica, *J. Chem. Phys.* 59 (3) (1973) 1198.
- [21] P.L. Studt, J.F. Shackelford, R.M. Fulrath, Solubility of gases in glass—a monatomic model, *J. Appl. Phys.* 41 (1970) 2777.
- [22] J.F. Shackelford, P.L. Studt, R.M. Fulrath, Solubility of gases in glass. Part II. He, Ne, and H<sub>2</sub> in fused silica, *J. Appl. Phys.* 43 (1972) 1619.
- [23] S.T. Oyama, D. Lee, P. Hacıoğlu, R.F. Saraf, *J. Membr. Sci.*, in preparation.
- [24] J.E. Dennis Jr., R.B. Schnabel, Numerical Methods for Unconstrained Optimization and Nonlinear Equations, Prentice-Hall, Englewood Cliffs, New Jersey, 1983.
- [25] R.W. Lee, R.C. Frank, D.W. Swets, Diffusion of hydrogen and deuterium in fused quartz, *J. Chem. Phys.* 36 (1962) 1062.
- [26] R.W. Lee, Diffusion of hydrogen in natural and synthetic fused quartz, *J. Chem. Phys.* 38 (1963) 448.
- [27] J.E. Shelby, Helium migration in natural and synthetic vitreous silica, *J. Am. Ceram. Soc.* 55 (1972) 61.
- [28] J.E. Shelby, Temperature dependence of He diffusion in vitreous SiO<sub>2</sub>, *J. Am. Ceram. Soc.* 54 (1972) 125.
- [29] J.E. Shelby, Molecular diffusion and solubility of hydrogen isotopes in vitreous silica, *J. Appl. Phys.* 48 (1977) 3387.
- [30] J.E. Shelby, Pressure dependence of helium and neon solubility in vitreous silica, *J. Appl. Phys.* 47 (1976) 135.